Calcium Clearance Mechanisms of Mouse Sperm

Gunther Wennemuth,[1,2] Donner F. Babcock,[1] and Bertil Hille[1]

[1]Department of Physiology and Biophysics, University of Washington, Seattle, WA 98195

[2]Department of Anatomy and Cell Biology, Philipps University Marburg, 35037 Marburg, Germany

ABSTRACT The spermatozoon is specialized for a single vital role in fertilization. Past studies show that Ca^{2+} signals produced by the opening of plasma membrane entry channels initiate several events required for the sperm to reach and enter the egg but reveal little about how resting $[Ca^{2+}]_i$ is maintained or restored after elevation. We examined these homeostatic mechanisms by monitoring the kinetics of recovery from depolarizing stimuli under conditions intended to inhibit candidate mechanisms for sequestration or extrusion of Ca^{2+} from the cytosol. We found that the Ca^{2+}-ATPase pump of the plasma membrane performs the major task of Ca^{2+} clearance. It is essential in the final stages of recovery to achieve a low resting $[Ca^{2+}]_i$. With immunomethods we found a $\sim$130-kD plasma membrane Ca^{2+}-ATPase protein on Western blots of whole sperm extracts and showed immunolocalization to the proximal principal piece of the flagellum. The plasma membrane Na^+-Ca^{2+} exchanger also exports Ca^{2+} when $[Ca^{2+}]_i$ is elevated. Simultaneous inhibition of both mechanisms of extrusion revealed an additional contribution to clearance from a CCCP-sensitive component, presumably sequestration by the mitochondria. Involvement of SERCA pumps was not clearly detected. Many aspects of the kinetics of Ca^{2+} clearance observed in the presence and absence of inhibitors were reproduced in a mathematical model based on known and assumed kinetic parameters. The model predicts that when cytosolic $[Ca^{2+}]$ is at $1\ \mu M$, the rates of removal by the Ca^{2+}-ATPase, Na^+-Ca^{2+}-exchanger, mitochondrial uniporter, and SERCA pump are $\sim$1.0, 0.35, 0.33, and 0 μmole l^{-1} s^{-1}, rates substantially slower than those reported for other cells studied by similar methods. According to the model, the Na^+-Ca^{2+} exchanger is poised so that it may run in reverse at resting $[Ca^{2+}]_i$ levels. We conclude that the essential functions of sperm do not require the ability to recover rapidly from globally elevated cytosolic $[Ca^{2+}]$.

KEY WORDS: Ca^{2+}-transporting ATPase • calcium uniporter • sodium-calcium exchanger • PMCA • SERCA

INTRODUCTION

Like other excitable cells, mammalian spermatozoa apparently possess multiple voltage-gated calcium channels and use Ca^{2+} signals to control physiological responses (Babcock and Pfeiffer, 1987; Darszon et al., 1999; Publicover and Barratt, 1999; Ren et al., 2001). Calcium is considered a regulator of sperm motility, a participant in capacitation, and an essential second messenger for the acrosome reaction. Indeed, one popular hypothesis concerning the response of sperm to contact with glycoproteins of the egg zona pellucida is reminiscent of secretory signaling in neurons and endocrine cells. In this view, the sperm plasma membrane depolarizes, Ca^{2+} channels open, Ca^{2+} enters, and the Ca^{2+}-dependent acrosome reaction ensues (Darszon et al., 1999). A variant of this model invokes release of Ca^{2+} from putative intracellular stores, followed by a prolonged phase of stores-operated Ca^{2+} entry from the outside (O'Toole et al., 2000; Jungnickel et al., 2001). Most of the work on Ca^{2+} dynamics in sperm has focused on mechanisms of Ca^{2+} entry.

This paper examines the clearance mechanisms. How do mature sperm maintain a low resting $[Ca^{2+}]_i$ despite an inevitable slow ongoing leak of Ca^{2+} into the cell, and how do they remove Ca^{2+} following an elevation of $[Ca^{2+}]_i$?

Four major Ca^{2+} clearance mechanisms are found in most animal cells, two on the plasma membrane and two on intracellular organelles. They have been studied best in nerve, muscle, and endocrine cells. The plasma membrane Ca^{2+}-ATPase (PMCA)* exports a cytoplasmic Ca^{2+} ion and imports one or two extracellular protons at the expense of ATP. Hence, it can be slowed by lowering the extracellular proton concentration, i.e., by raising the pH of the bath (Xu et al., 2000). It also is blocked from the cytoplasmic side by eosin analogs (Gatto and Milanick, 1993) and from the outside by submillimolar concentrations of La^{3+} (Shimizu et al., 1997). When $[Ca^{2+}]_i$ is elevated, the plasma membrane Na^+-Ca^{2+} exchanger (NCX) operating in forward mode exports an intracellular Ca^{2+} ion

Abbreviations used in this paper: CCCP, carbonylcyanide-*m*-chlorophenylhydrazone; CPA, cyclopiazonic acid; MCU, mitochondrial Ca^{2+} uniporter; NCKX, sodium-calcium-potassium exchanger; NCX, Na^+-Ca^{2+} exchanger; PMCA, plasma membrane Ca^{2+}-ATPase; SERCA, sarco-endoplasmic reticulum Ca^{2+}-ATPase.

and imports approximately three Na^+ ions at the expense of the Na^+ gradient (Blaustein and Lederer, 1999; Philipson and Nicoll, 2000). The direction of the exchange can be reversed either by depolarizing the cell or by removing extracellular Na^+, for example by replacing it with Li^+. The best-known organellar clearance mechanism is the sarcoplasmic-endoplasmic reticulum Ca^{2+}-ATPase (SERCA pumps; MacLennan et al., 1997). SERCA pumps are inhibited by thapsigargin and cyclopiazonic acid. In addition, the mitochondrial Ca^{2+} uniporter (MCU) brings Ca^{2+} into energized mitochondria when $[Ca^{2+}]_i$ is elevated above $\sim$500 nM (Gunter et al., 2000). Net Ca^{2+} uptake via the MCU stops when the electrical driving force across the inner mitochondrial membrane is collapsed by protonophores (uncouplers) such as CCCP. Collapse of the mitochondrial membrane potential also stops mitochondrial ATP synthesis.

The relative importance of the different Ca^{2+} clearance mechanisms has been explored quantitatively in only a few cell types. Among the cells studied, both the balance of components and their absolute rates differ. In the squid giant axon, the PMCA is considered the most important mechanism for maintaining the low resting $[Ca^{2+}]_i$ level (DiPolo and Beauge, 1983). It has the highest Ca^{2+} affinity and it exports Ca^{2+} into the external medium. The NCX has lower affinity, but often a higher capacity. For example, in cardiac muscle, the NCX returns considerable quantities of Ca^{2+} ions to the extracellular medium during each cardiac cycle (Blaustein and Lederer, 1999; Weber et al., 2001). In skeletal muscle, the dominant Ca^{2+} clearance after each twitch is via SERCA pumps on the sarcoplasmic reticulum (Klein et al., 1991). The clearance is fast, taking only a fraction of a second. In chromaffin cells, the Ca^{2+} accumulation in mitochondria via the MCU is the fastest clearance mechanism when $[Ca^{2+}]_i$ is elevated, but this Ca^{2+} sequestration is only transient (Herrington et al., 1996; Babcock et al., 1997). Mitochondria return their Ca^{2+} load to the cytoplasm once $[Ca^{2+}]_i$ is lowered, and eventually the PMCA does the final job of clearing Ca^{2+} ions from the chromaffin cell and setting the low, resting $[Ca^{2+}]_i$.

In this paper we dissect the Ca^{2+} clearance mechanisms of sperm both pharmacologically and by changing the ion content of the medium. We repeatedly introduce Ca^{2+} loads into the cytoplasm by short KCl depolarizations of the sperm membrane and follow the time course of $[Ca^{2+}]_i$ recovery using fluorescent Ca^{2+} indicators. This allows us to compare clearance in different media designed to depress one or several of the candidate transport mechanisms. One motivation for these studies is that a better understanding of Ca^{2+} regulation could suggest approaches to regulating the reproductive success of spermatozoa.

MATERIALS AND METHODS

Materials

Pluronic F127 and indo-1 AM were from Molecular Probes; thapsigargin, cyclopiazonic acid (CPA), and carbonylcyanide-*m*-chlorophenylhydrazone (CCCP) were from Calbiochem. All other chemicals were from Sigma-Aldrich. Nitrocellulose membranes, MES-SDS running buffer, transfer buffer, reducing agent, and Bis-Tris precast gels were from Invitrogen. Chemiluminescence detection kits were from Pierce Chemical Co. Antibody against PMCA (clone 5F10) was from Upstate Biotechnology. Secondary antibodies were from Santa Cruz Biotechnology, Inc. Chamber slides with covers were from Nalge Nunc International and Vectashield mounting medium was from Vector.

Solutions and Preparation of Sperm

The caudae epididymides and vasa deferentia were excised from mice (Swiss Webster, retired breeders killed by CO_2 asphyxiation) and cleaned in medium Na7.4 (in mM): 135 NaCl, 5 KCl, 1 $MgCl_2$, 2 $CaCl_2$, 30 HEPES, 10 glucose, 10 lactic acid, 1 pyruvic acid, adjusted to pH 7.4 with NaOH. The tissue was transferred to 1 ml medium Na7.4 containing 5 mg BSA and 15 mM $NaCO_3$ and incised 5–10 times to allow sperm to exude into the medium (15 min, 37°C, 5% CO_2). All following steps were done with bicarbonate-free medium Na7.4 and at room temperature, unless otherwise noted. Sperm were washed twice by diluting to 2 ml and centrifuging (400 *g*, 3 min). The final concentration for storage was 1–2 × 10^7 cells/ml.

Ca^{2+} clearance was studied during recovery from depolarization-induced elevations of intracellular $[Ca^{2+}]$. Ca^{2+} entry was evoked by 10-s applications of the alkaline, high K^+ solution K8.6 (in mM): 135 KCl, 5 NaCl, 1 $MgCl_2$, 2 $CaCl_2$, 10 glucose, 10 lactic acid, 1 pyruvic acid, 30 TAPS; adjusted to pH 8.6 with KOH. The high K^+ of this medium depolarizes the cell and opens voltage-gated Ca^{2+} channels, and the high pH augments the rise of $[Ca^{2+}]_i$ (Wennemuth et al., 2000). During the subsequent measurements of Ca^{2+} clearance, sperm were bathed in test solutions adjusted to different pH values (7.4 or 8.6) with either Na^+ or Li^+ as the principal cation. These test solutions were designated Na7.4, Na8.6, Li7.4, and Li8.6, Li7.4, and Li8.6 were made by replacing all Na^+ salts with Li^+. Likewise, NaCCP7.4 is Na7.4 containing 2 μM CCCP.

Conditioning with sodium bicarbonate potentiates Ca^{2+} entry during KCl depolarization (Wennemuth et al., 2000, 2003). It also increases production of cyclic AMP, enhances the motility of sperm (Okamura et al., 1985; Wennemuth et al., 2003), and, with long exposures, promotes capacitation (Visconti et al., 1995). Sodium bicarbonate (15 mM) was added to the Na7.4 solution where stated to make solution NaB7.4. Solution NaB7.4 was used as the control solution during the Ca^{2+} clearance to maintain large Ca^{2+} entries in each trial.

Dye Loading and Photometry

We followed previously described protocols for loading of sperm samples with indo-1 AM, for ratio-photometric measurements of $[Ca^{2+}]_i$, and for rapid local application of test solutions (Herrington et al., 1996; Wennemuth et al., 2000). Control experiments showed that solutions were exchanged in <800 ms. As a criterion of cell quality, we used only those sperm that remained motile throughout the experiment. The photometric measurements were made on small clusters of 4–6 cells adhering to 5 × 5 mm square glass coverslips. Although the flagella continued to beat, the sperm heads adhered to the coverslip, and their image remained within the 25-μm diameter area monitored by the pho-

tomultiplier detectors. Thus, we measure primarily light from the sperm head and midpiece, and our measurements should reflect the spatially averaged $[Ca^{2+}]_i$ there. The photometric signals were corrected for background fluorescence and calibrated with the constants R_{min} (1.067), R_{max} (6.488), and K^* (1470 nM) obtained from cells equilibrated in solutions that contained ionomycin (10 µM) and either 50 mM EGTA, or 15 mM $CaCl_2$, or 20 mM EGTA with 15 mM $CaCl_2$ (calculated free $[Ca^{2+}]$ of 251 nM).

To cast our Ca^{2+} measurements in terms of molar Ca^{2+} flux densities across the plasma membrane required knowledge of the Ca^{2+} binding ratio (bound calcium/free calcium) in the cytoplasm. Because the indo-1 in sperm could contribute substantially as a Ca^{2+} buffer, we determined its cytoplasmic concentration. The approach was to use a conventional fluorometer (SLM-Aminco SPF 500) to compare optical properties of suspensions of sperm that were loaded with indo-1 a.m. to those of sperm-free solutions containing known concentrations of authentic indo-1. To maximize the similarities in the conditions of comparison, we determined maximal emission intensities from spectral scans of the Ca^{2+}-saturated dye in vitro and in vivo. Loaded sperm were incubated for 2 h in Na7.4 to promote complete hydrolysis of the intracellular indo-1 AM ester, sedimented, and resuspended in fresh Na7.4. This wash removed extracellular indo-1 nearly completely, as indicated by the minimal immediate decrease in fluorescence produced in a parallel experiment by the addition of 20 µM $MnCl_2$. Fluorescence excitation spectra (300–400 nm; 410 nm emission) and emission spectra (400–600 nm with 350 or 365 nm excitation) of the cell suspension were determined immediately after washing and again 2 min after addition of 5 µM ionomycin (with 2 mM external Ca^{2+}) to saturate the internal dye with Ca^{2+}. A final scan was collected 2 min after a subsequent addition of 20 µM $MnCl_2$ to quench indo-1 fluorescence completely. The residual Mn^{2+}-resistant signal presumably represents cellular autofluorescence and incompletely hydrolyzed indo-1 AM. It was subtracted from the signal of the suspensions that contained the Ca^{2+}-saturated intracellular dye. The peak intensity of this difference signal was equivalent to that of 25 nM indo-1 examined in vitro in an "intracellular" buffer (120 mM KCl, 10 mM NaCl, 1 mM $MgCl_2$, 10 mM HEPES adjusted to pH 7.4 with NaOH) supplemented with 2 M sucrose and 1 mM $CaCl_2$. From a direct determination of the cell concentration in the sperm suspension (3×10^6 ml^{-1} by a hemocytometer count) and the reported water volume of 43 fl for the mouse spermatozoon (Du et al., 1994), we calculated an intracellular indo-1 concentration of 340 and 420 µM in two independent experiments.

Immunocytochemistry

Aliquots (100 µl) of the sperm suspension were placed in chamber slides and allowed to settle for 15 min. Adherent sperm were gently washed twice with PBS and fixed with 4% paraformaldehyde and 5% methanol (15 min). Cells were permeabilized with 0.5% Triton X-100 in PBS for 15 min, and washed in PBS containing 5% BSA (5×5 min). Slides were incubated with primary antibody (diluted in PBS containing 5% BSA) overnight at 4°C, washed in PBS (5×5 min), and incubated 1 h with a Cy3-labeled secondary antibody. Samples were washed in PBS (3×5 min) and then protected with DAPI-containing Vectashield mounting medium and coverslips. To check the specificity of primary antibody binding, we incubated control slides with the secondary antibody only. Fluorescence was observed by confocal imaging (Leica TCS SP/MP) at the Keck Imaging Facility of the University of Washington.

Immunoblots

Total proteins from mouse sperm were extracted by adding an equal volume of a 2× Laemmli buffer (Laemmli et al., 1970). Af-

ter heating for 5 min at 100°C, the samples were clarified by centrifugation at 5,000 *g* for 5 min and adjusted to 5% mercaptoethanol. Proteins were separated on a 4–12% gradient SDS-PAGE gel and transferred onto nitrocellulose membranes. Prior to the incubation with antibodies, nonspecific binding was blocked with PBS containing 5% (wt/vol) dried nonfat milk for 1 h. Blots were incubated with the primary antibody in dilutions from 1:500 to 1:8,000 for 1 h and washed with 0.1% Tween in PBS (4×5 min). Under the same conditions, blots were then incubated with horseradish peroxidase-labeled secondary antibody diluted 1:2,000 in PBS. Finally, blots were washed with 0.1% Tween in PBS (4×5 min) and treated with enhanced chemiluminescence detection reagents for 5 min.

Data Analysis

Analysis of photometric measurements and kinetic modeling were performed with Igor Pro (Wavemetrics) and Excel (Microsoft Corporation).

RESULTS

Measuring Ca^{2+} Clearance

Fig. 1 illustrates a typical protocol for studying Ca^{2+} clearance. It shows a 28-min record of spatially averaged $[Ca^{2+}]_i$ for a small cluster of sperm bathed most of the time in the bicarbonate-containing NaB7.4 solution. The calculated initial resting values for $[Ca^{2+}]_i$ are typically in the range of 100 to 250 nM. The cells are depolarized five times by 10-s applications of the K8.6 solution. Each time the $[Ca^{2+}]_i$ rises steeply (at 40–70 nM/s) by 400–700 nM during the depolarization and then begins to decay toward the baseline when the depolarizing solution is removed. The time course of this decay is our measure of Ca^{2+} clearance. In experiments published previously (Wennemuth et al., 2000, 2003), we found that the rate of Ca^{2+} rise, the peak $[Ca^{2+}]_i$ reached, and the subsequent "baseline" $[Ca^{2+}]_i$ level grew with repeated depolarizations, a phenomenon we called run-up. The growth in these values usually slowed by the third or fourth depolarization. In Fig. 1, the first Ca^{2+} elevation is small, the next one is larger, and then the growth stops. The baseline $[Ca^{2+}]_i$ level also increases relative to its value at the beginning of the experiment. After the first elevation, the time course of decay is relatively invariant. Single exponential curves fitted to the recovery time courses for the second through fifth depolarizations have time constants of 43, 48, 50, and 42 s, respectively, in this experiment.

Our standard protocol applies bicarbonate-free test solutions designed to inhibit specific components of Ca^{2+} clearance during recovery from the fourth depolarization. The clearance in NaB7.4 solution after the third elevation serves as a control for the test clearance after the fourth, and the clearance after the fifth elevation serves as an additional indicator of reversibility. In Fig. 1, depolarizations number 1, 2, 3, and 5 are followed by bicarbonate-containing NaB7.4, whereas the

FIGURE 1. Calcium clearance does not require external HCO_3^-. Elevations of $[Ca^{2+}]_i$ were elicited five times by 10-s depolarizations with the alkaline K^+-based medium K8.6 (as marked). During recovery, cells were returned routinely to the bicarbonate-containing medium NaB7.4 to maintain strong responses to the depolarizing stimulus. But after the fourth stimulus, they were returned to medium Na7.4 that lacks HCO_3^-.
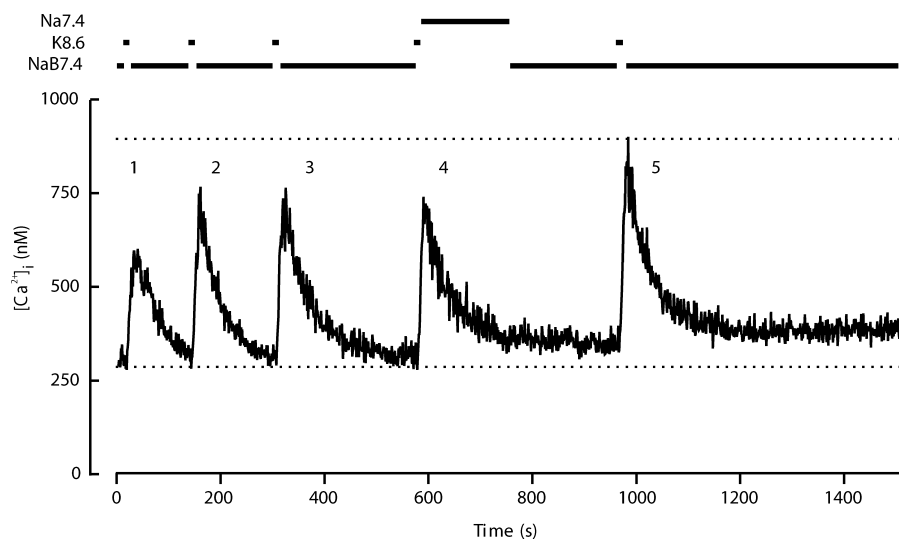
test recovery solution after depolarization 4 is bicarbonate-free Na7.4. This control experiment and five others like it showed that removing bicarbonate from the recovery solution did not change Ca^{2+} clearance. In subsequent experiments, bicarbonate was present in the control solution but absent from the depolarizing medium K8.6 and from all test recovery solutions, to pre-

clude complications associated with variations in medium pH over the range 7.4–8.6.

Two Plasma-membrane Ca^{2+} Transporters Dominate Rapid Ca^{2+} Clearance

Fig. 2 A shows an experiment to test the role of the PMCA. The cells are depolarized five times in K8.6, and

FIGURE 2. Slowing of the plasma membrane Ca^{2+}-ATPase by elevating pH$_o$ from 7.4 to 8.6 impairs Ca^{2+} clearance and $[Ca^{2+}]_i$ homeostasis. (A) Five 10-s depolarizing stimuli with K8.6 were applied as in Fig. 1. Recovery was monitored in medium NaB7.4 after stimuli 1, 2, 3, and 5, but for the fourth stimulus, the medium was changed to the alkaline solution Na8.6 during recovery. At the end of the experiment, Na8.6 was applied transiently for 170 s without a preceding depolarization in K8.6. (B) Simulations of the experiment in A using a kinetic model described in the APPENDIX and in Fig. 9 A. For this simulation only, two of the model parameters were adjusted. The parameter $M_{\text{leak in KCl}}$ was increased to 57 times $M_{\text{leak at rest}}$, and the set point (rest level) for intracellular $[Na^+]_i$ was progressively incremented after each KCl exposure. The initial value was 8 mM, and the subsequent values were 13.3, 16, 17.2, 17.6, and 18 mM.
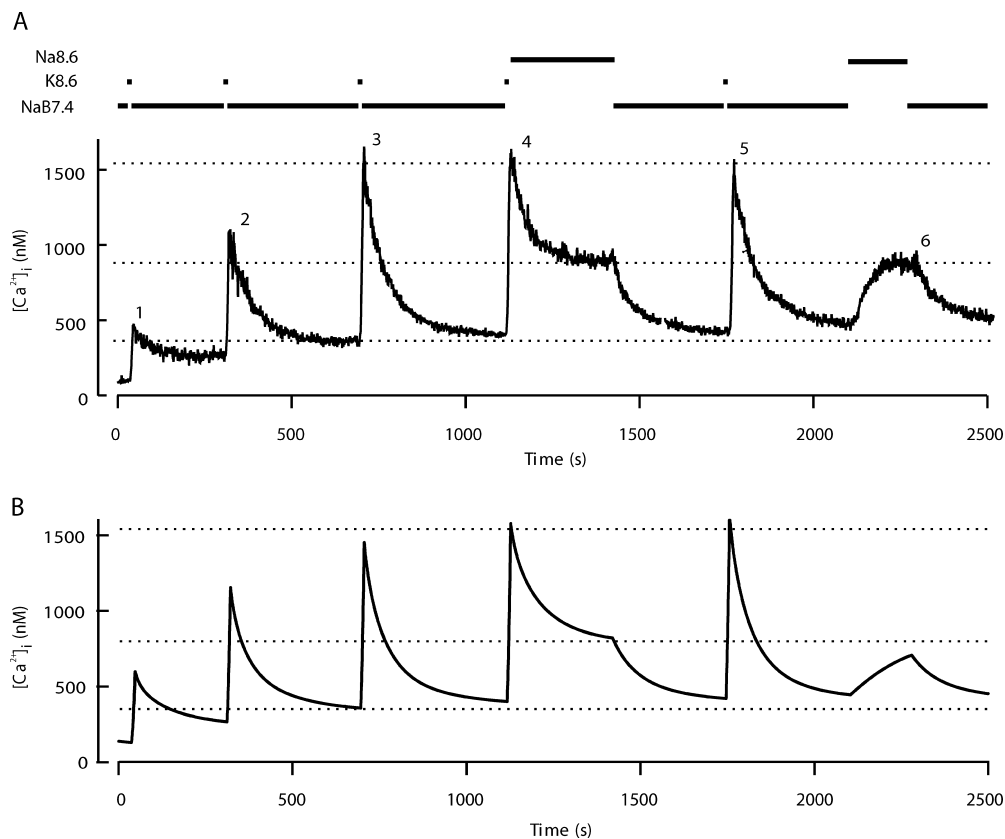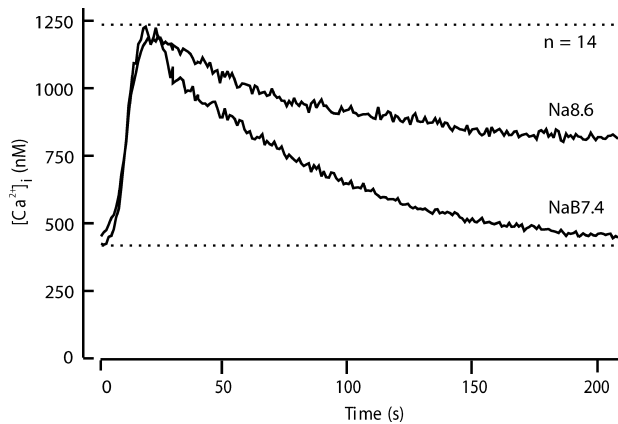
FIGURE 3. Comparison of calcium clearance with and without slowing of the plasma membrane Ca^{2+}-ATPase by alkaline pH_o. Recovery was monitored in 14 experiments with different cells using the five-stimulus protocol of Fig. 2. The records for the third (NaB7.4) and fourth (Na8.6) cycles of stimulus and recovery were aligned and averaged.

the decay in NaB7.4 solution after the third depolarization serves as the control. After the fourth depolarization, the solution is changed to a Na^+-containing alkaline medium (Na8.6), which should slow the PMCA because protons are an obligate substrate (Xu et al., 2000). At pH 8.6 the decreased proton concentration (2.5 nM) would slow the PMCA of red blood cells to 21% of its pH 7.4 value (Xu et al., 2000). In the experiment here the initial rate of fall of $[Ca^{2+}]_i$ is depressed in Na8.6 solution, and the $[Ca^{2+}]_i$ reaches a plateau at a much elevated level. The effects are fully reversible. Upon return to NaB7.4 solution, the excess Ca^{2+} is quickly cleared and the full time course of clearance is normal after the fifth depolarization. At the end of the experiment, switching to the Na8.6 solution without any prior depolarization causes $[Ca^{2+}]_i$ to rise reversibly from its baseline to the same elevated plateau value. These observations are simulated in Fig. 2 B with a model described later.
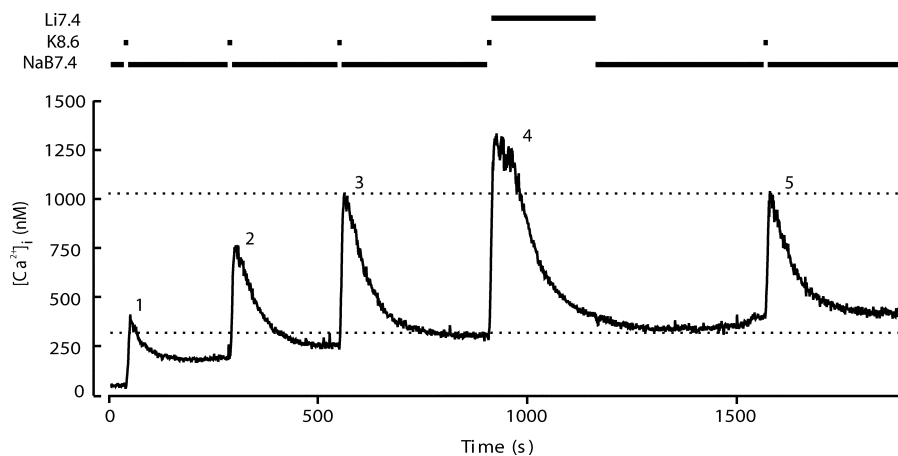
Fig. 3 extends these observations by comparing the mean time course of decay in 14 similar experiments. High pH slows net Ca^{2+} clearance at high values of $[Ca^{2+}]_i$ by 60% and makes the recovery incomplete. In the Na8.6 solution, net Ca^{2+} clearance stops at $\sim$850 nM Ca^{2+} instead of bringing Ca^{2+} to below 400 nM. Evidently the PMCA is necessary to achieve the normal low resting level of $[Ca^{2+}]_i$. When the PMCA is depressed, other mechanisms can clear cytoplasmic Ca^{2+} only to an intermediate level in the face of an ongoing background leak.

Fig. 4 shows a similar experiment to test the importance of the NCX for Ca^{2+} clearance. Here switching to a Na^+-free solution (Li7.4) again alters Ca^{2+} clearance, and recovery is retarded compared with the control. The average of 10 experiments in Fig. 5 shows that the changes in time course in Li7.4 are different from those for Na8.6. Instead of starting to fall at once, $[Ca^{2+}]_i$ continues to grow for >10 s after the depolarizing K8.6 solution is replaced by Li7.4. The peak $[Ca^{2+}]_i$ that is reached in Li7.4 is well above that seen with Na7.4. Nevertheless, $[Ca^{2+}]_i$ eventually recovers almost to the previous resting level despite the continued absence of external Na^+ to run the NCX in the forward (Ca^{2+} efflux) mode. We suggest later that $[Ca^{2+}]_i$ continues to rise in Li7.4 for a while, because in the absence of external Na^+ the NCX operates transiently in reverse mode, taking Ca^{2+} into the sperm in exchange for internal Na^+. Such reverse operation would stop as the intracellular Na^+ becomes depleted. Evidently a significant NCX is present. Its forward operation is most obvious at supramicromolar levels of $[Ca^{2+}]_i$, whereas when $[Ca^{2+}]_i$ is below 500 nM, the PMCA is the dominant clearance mechanism. The effects of Li7.4 were fully reversed by returning to Na7.4.

We have attributed the exchange of Na^+ for Ca^{2+} to transport by a classical NCX transporter. Indeed by RT-PCR, two splice variants, NCX1.3 and 1.7, of the NCX1 gene are reported in rat testis (Quednau et al., 1997). By way of caution, we note that a Na^+-Ca^{2+}-K^+ exchanger

FIGURE 4. Interfering with the plasma membrane Na^+-Ca^{2+} exchanger allows slow but complete recovery from evoked Ca^{2+} entry. Five depolarizing stimuli with K8.6 were applied as in Fig. 1. Recovery was monitored in medium NaB7.4 after stimuli 1, 2, 3, and 5. After the fourth stimulus, the medium was changed to Li7.4 to examine recovery in the absence of external Na^+, an essential substrate for forward-mode operation of the NCX.
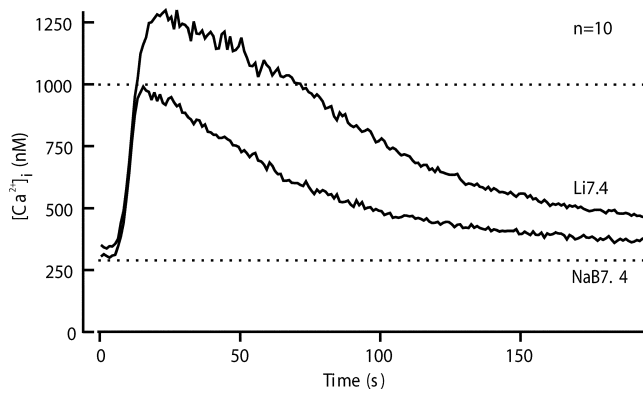
FIGURE 5. Comparison of calcium clearance with and without Na$^+$ in the external medium to test the contribution of the Na$^+$-Ca^{2+} exchanger. Recovery was monitored in 10 experiments using a five-stimulus protocol of Fig. 4. The traces for the third (NaB7.4) and fourth (Li7.4) cycles of stimulus and recovery were aligned and averaged.

FIGURE 6. Comparison of calcium clearance with and without simultaneous inhibition of the plasma membrane Na$^+$-Ca^{2+} exchanger (NCX) and the Ca^{2+}-ATPase pump (PMCA). Recovery was monitored in 14 experiments using a five-stimulus protocol as in Figs. 2 and 4. The traces for the third (NaB7.4) and fourth (Li8.6) cycles of stimulus and recovery were aligned and averaged.

(NCKX), would also reverse direction in Na$^+$-free solutions. Although the NCKX was first discovered in photoreceptors, mRNAs for various isoforms are found in other tissues. By RT-PCR, message for the NCKX3 isoform is found in mouse testis (Kraev et al., 2001), and by cloning, immunocytochemistry, and flux experiments an NCKX is important for Ca^{2+} regulation in sea urchin sperm (Su and Vacquier, 2002). Seeking evidence of operation of a NCKX in mouse sperm, we repeated the experiments with Li7.4 recovery solutions, comparing recovery in the standard version containing 2.5 mM K$^+$ with that in another version lacking K$^+$. The latter solution would not allow reverse-mode operation of a NCKX. Since the recovery time courses were indistinguishable in the two Li7.4 solutions (unpublished data, $n = 11$), the NCX probably accounts for most of the Na$^+$-dependent exchange.

Synergy of the PMCA and the NCX in Ca^{2+} clearance is emphasized in experiments using an alkaline, Na$^+$-free solution (Li8.6) that should affect both of them (Fig. 6). In this solution the impairment of Ca^{2+} clearance is extreme. Again with this Na$^+$-free solution, the [Ca^{2+}]$_i$ first continues to rise after K8.6 is removed, but then the decline of [Ca^{2+}]$_i$ is so slow in Li8.6 that after 150 s it is still near 1,000 nM. In contrast, in the control Na7.4 solution full recovery occurs by this time.

We have interpreted the effects of high pH solutions as a simple slowing of the PMCA, and indeed elevated pH does inhibit the PMCA (by as much as 95% at pH 10.2; Xu et al., 2000), whereas the effect of pH elevation to pH 9.0 on three expressed isoforms of mammalian NCX is slight and stimulatory (Linck et al., 1998). Nevertheless, high pH is a nonspecific treatment that might have effects on other Ca^{2+} transporters and buffers. Therefore, we checked for intracellular pH changes and tried two other approaches to inhibiting

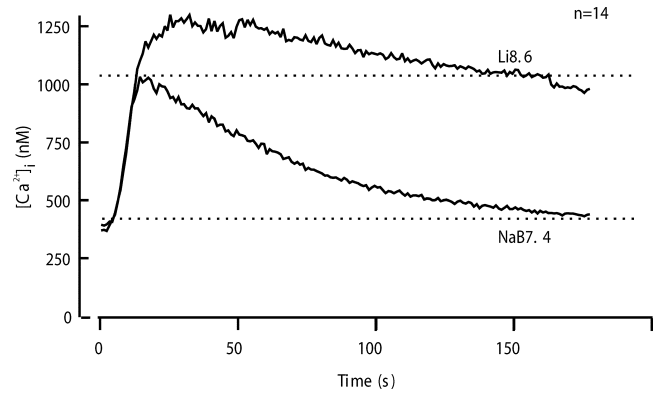plasma membrane Ca^{2+} transporters. Control experiments with the pH indicator BCECF showed that intracellular pH changes were small during exposures to the pH 8.6 external solutions. The pH rose by only ∼0.1 U (from 7.0 to 7.1) during 10 s in K8.6 ($n = 54$). The pH did not change further on switching to Na8.6 for 120 s ($n = 17$), but did return slowly ($\tau = 38$ s) to rest on switching to Na7.4 ($n = 20$) or Li7.4 ($n = 17$) for 120 s. Any residual offset of intracellular pH was corrected within 20 s in NaB7.4, sometimes with a transient acidic overshoot. We tried two other approaches to blocking the PMCA. One was intracellular carboxyeosin, which was preloaded for 15 min as the diacetyl ester (20 μM) at the same time as indo-1, followed by the usual 1–3 h wait for cleavage of the ester forms before the experiment started. We anticipated that inhibition of the PMCA by carboxyeosin would produce results similar to treatments with Na8.6 without a prior K8.6 challenge (Fig. 2). Indeed, the intracellular carboxyeosin caused Ca^{2+} to rise to 800–1,000 nM ($n = 9$). However, these cells, whose [Ca^{2+}]$_i$ had been elevated for >1 h, no longer responded well to KCl depolarizations for additional clearance studies. We also tested the action of 30 μM La^{3+}, which at this low concentration should block the PMCA and possibly slow the NCX (Shimizu et al., 1997). When La^{3+} was applied immediately after a standard K8.6 depolarization, the [Ca^{2+}]$_i$ trajectory was like that in Li8.6 for 30 s but the optical signal then continued to rise gradually as if La^{3+} was entering slowly and binding to the indo-1 reporter. These cells also lost their motility irreversibly, consistent with entry of La^{3+}.

Sperm Mitochondria Can Take Up Ca^{2+}

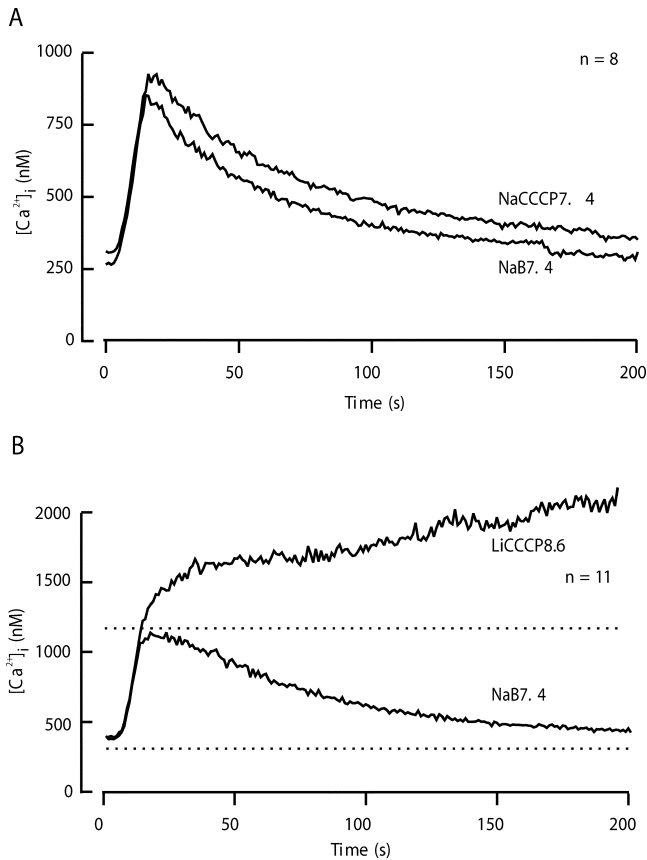Together, the PMCA and the NCX are dominant routes of Ca^{2+} clearance in sperm. Nevertheless, some resid-

A

B

FIGURE 7. Prevention of Ca^{2+} sequestration by mitochondria alters Ca^{2+} clearance only a little, but reveals a background Ca^{2+} leak. Recovery was monitored in two kinds of experiments using a five-stimulus protocol (as in Figs. 2 and 4) with test solutions containing 2 μM CCCP. The records for the third (Na7.4) and fourth (test) cycles of stimulus and recovery were aligned and averaged. (A) Test solution, NaCCCP7.4 (ν = 8). (B) Test solution, LiCCCP8.6 (n = 11).

ual clearance mechanism still operates in Li8.6 because $[Ca^{2+}]_i$ falls slowly from the 1,250 nM peak in the cytoplasm, despite the much higher (2 mM) level in the extracellular medium. Mitochondria offer an organellar route for Ca^{2+} clearance. Fig. 7 A compares the mean time course of clearance in the Na7.4 control solution with that in the NaCCCP7.4 solution designed to depolarize the inner mitochondrial membrane and prevent Ca^{2+} uptake by the MCU. These experiments show that blocking mitochondrial uptake alone has a minor effect on total clearance, retarding recovery only a small amount. However, when CCCP is applied together with Li8.6, the situation is different. In the LiCCCP8.6 solution, no net Ca^{2+} clearance occurs after the depolarizing pulse (Fig. 7 B). Instead, the $[Ca^{2+}]_i$ continues to climb slowly above 1,500 nM. Hence, 2 μM CCCP blocks a component of Ca^{2+} clearance that operates at high values of $[Ca^{2+}]_i$ and is revealed when the two dominant, plasma-membrane mechanisms are blocked.

The combination of three inhibitors in LiCCCP8.6 solution reveals a net inward leak of Ca^{2+}.

Experiments with SERCA Pump Inhibitors Are Ambiguous

In many cell types at rest, a large intracellular Ca^{2+} store in the ER is in a dynamic steady-state with cytoplasmic Ca^{2+}. Often the continuous turnover of Ca^{2+} in the ER is so large that cytoplasmic Ca^{2+} will rise quickly after sudden addition of thapsigargin or cyclopiazonic acid to block SERCA pumps. In sperm, neither thapsigargin nor cyclopiazonic acid gives a rapid elevation of $[Ca^{2+}]_i$, suggesting either that ER stores are small or empty and/or that the resting efflux from stores is smaller than in most cells. Nevertheless, $[Ca^{2+}]_i$ does rise gradually when the inhibitors are added. With thapsigargin (3 μM), the effect is irreversible and is accompanied by loss of sperm motility. The $[Ca^{2+}]_i$ starts to rise at ~2 nM/s, leveling off after an increment of 100–200 nM, and cellular motility ceases within a couple of minutes. Such actions precluded meaningful study of clearance. With cyclopiazonic acid (25 μM), there was a similar slow rise of $[Ca^{2+}]_i$ followed by a leveling, but the effect was at least partially reversible. Motility was only partly depressed, and it improved slowly after the inhibitor was removed. Net Ca^{2+} clearance after a depolarization was not appreciably changed by using a 2-min preincubation in Na7.4-containing cyclopiazonic acid and switching back to this cyclopiazonic acid–containing solution for the recovery (unpublished data). Thus, SERCA pumps are not a major component of Ca^{2+} clearance in response to KCl depolarization.

Immunocytochemistry

We wished to map the subcellular localization of the PMCA pumps in mouse sperm. In the top panel of Fig. 8 a brightfield image of a mouse spermatozoon is shown both alone and overlain by outlines defining the major regions of these cells. The bottom panels show representative composite immunofluorescence and nuclear fluorescence images for cells stained with antibodies directed toward the PMCA (Fig. 8 C). The PMCA labeling appears in patches along the principal piece of the tail (white arrow), whereas the midpiece and the head are unlabeled. The staining tapers off distally toward the tip of the flagellum. Fig. 8 D shows that Western blot analysis of whole mouse sperm extracts using the PMCA antibody detects a band at ~130 kD, as is expected for authentic PMCA protein.

Model

Our experiments revealed involvement of at least three Ca^{2+} clearance mechanisms in sperm. To evaluate their relative importance, we made a quantitative model that simulated the time course of Ca^{2+} entry and clearance.
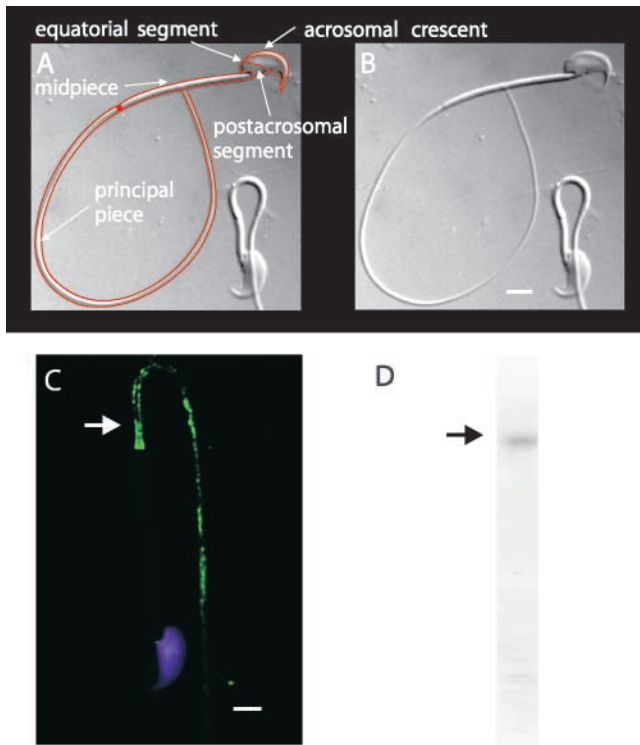
FIGURE 8. Subcellular localization of plasma membrane Ca^{2+}-ATPase in sperm. (A and B) DIC images of mouse sperm. In A, a line drawing overlays the image and arrows designate major anatomical features. (C) Sperm stained with the nuclear stain DAPI (blue) and anti-PMCA primary antibody (green). Immunoreactivity was found exclusively in the principal piece of the flagellum (arrow). Bars, 3 μm. (D) Western immunoblots indicate a major immunoreactive protein band migrating near that of a 140-kD marker protein (arrow).

The model contained rate laws for three Ca^{2+} clearance mechanisms: the PMCA, NCX, and MCU, and a leak for Ca^{2+} entry. The rate equations and affinity constants were taken mostly from similar published models for other mammalian cell types and are given in the APPENDIX. Although spermatozoa have an extended geometry and their channels and transporters have distinct subcellular distributions, the simple model given here, like our measurements, assumes a single, well-stirred cytoplasmic compartment.

The PMCA rate law was the product of two simple Michaelis-Menten saturation functions, with dissociation constants K_{Ca} of 550 nM (Weber et al., 2001) and K_H of 13.7 nM ($pK_a = 7.86$) (Xu et al., 2000) for activation by intracellular Ca^{2+} and by extracellular protons, respectively. With a pK_a of 7.86, the PMCA would be 4.8-fold slower at external pH 8.6 than at pH 7.4. The NCX rate law was a complex empirical expression taken from Weber et al. (2001; their Eq. 1) for mouse heart. This expression, reminiscent of a Goldman-Hodgkin-Katz current equation, has a reversal potential appropriate for an electrogenic process exchanging 3

Na^+ ions for 1 Ca^{2+} ion and fluxes governed by the saturation of the transport sites. An alternative mechanistic equation, provided by Dr. Donald Hilgemann, gave similar results and was equally satisfactory. It was derived from the kinetics of an exchanger with sequential loading of unequal sites (compare Matsuoka and Hilgemann, 1992). The MCU was represented as a device with no transport when $[Ca^{2+}]_i < 450$ nM, and a linear increase in uptake velocity for higher values of $[Ca^{2+}]_i$ (compare Fig. 6 in Herrington et al., 1996). Export of Ca^{2+} from mitochondria was not included in the model. Experiments described in Methods determined the intracellular indo-1 concentration in two batches of sperm, giving 340 and 420 μM. The intracellular Ca^{2+}-binding ratio (buffer) therefore was modeled as the effect of 380 μM indo-1 plus an assumed fixed endogenous value of 100 (compare Neher and Augustine, 1992; Herrington et al., 1996). The indo-1 more than doubles the binding ratio in part of the calcium range of interest. Thus, the assumed endogenous buffer contributes a binding ratio of 100, and the indo-1 contributes an additional binding ratio of 376, 156, 85, and 54 at Ca^{2+} concentrations of 250, 500, 750, and 1,000 nM, respectively.

In addition, since the NCX exports Na^+ ions from a limited pool in the cytoplasm when running backward, we had to represent changes in cytoplasmic Na^+ as well. We assumed that for every Ca^{2+} moved by the NCX, three Na^+ ions move in the opposite direction. Intracellular Na^+ is otherwise regulated by a pump-leak system with a linear concentration dependence on intracellular Na^+ and a set point of 16.5 mM (compare 14 mM in Babcock, 1983) in Na^+-containing bathing media and a set point of 0 mM in Na^+-free solutions. The pump-leak rate was set so that $[Na^+]_i$ relaxed to new values with a time constant of 15 s. Control experiments (unpublished data) using the Na^+ indicator SBFI showed cytoplasmic Na^+ relaxation times in the 6–15 s range on switching from NaB7.4 to Na^+-free solutions and back.

The rates of the PMCA and NCX and the total fluxes of all mechanisms are estimated from our experimental observations in Table I. The second column is the observed rate of change of free $[Ca^{2+}]_i$ at 1,000 and 750 nM calcium levels (slope of clearance in Figs. 3, 5, and 6) in several test solutions after a depolarization. The third column is the change in slope relative to control (NaB7.4) induced by the Na8.6, Li7.4, and Li8.6 recovery solutions. The fourth column is the scaling factor needed to correct for calcium binding ratios and, in the case of Na8.6, for the incomplete inhibition of the PMCA by pH 8.6. The next column, the product of the two preceding, is our experimental estimate of the molar Ca^{2+} transport rates. The rates of the PMCA, NCX, and total flux in the model equations were then scaled

T A B L E I

Estimation of Molar Transport Rates from Changes of d[Ca²⁺]ᵢ/dt with Inhibitors

	Measured at 1,000 nM [Ca²⁺]ᵢ					Measured at 750 nM [Ca²⁺]ᵢ				
Solution	Observed d[Ca²⁺]/dt	Change of slope	Scaling factor	Molar flux	Transporter	Observed d[Ca²⁺]/dt	Change of slope	Scaling factor	Molar flux	Transporter
	nM/s	*nM/s*		*nM/s*		*nM/s*	*nM/s*		*nM/s*	
Na7.4	8	—	154	1,232	net	5.9	—	185	1,092	net
Na8.6	3.1	4.9	195	755	PMCA	—	—	—	—	—
Li7.4	6.5	1.5	154	231	NCX	6.2	0.3	185	56	NCX
Li8.6	1.2	−6.8	154	1,047	PMCA + NCX	—	—	—	—	—

Observed d[Ca²⁺]ᵢ/dt is the rate of change of free [Ca²⁺]ᵢ reported by indo-1 dye. Change of slope is the difference in slope between control (Na7.4) and listed test solutions. Scaling factor is the Ca²⁺ binding ratio or, for Na8.6, the binding ratio times 1.27 (see text). Molar flux is the product of scaling factor times change of slope, or for control solution, times observed d[Ca²⁺]ᵢ/dt.

to approximate these measured rates (Fig. 9 A). The APPENDIX gives the resulting assumed dependence of fluxes on [Ca²⁺]ᵢ.

Calculations of clearance time courses with the model were started from steady-state resting conditions and integrated in time steps of 0.5 s by the Euler method, assuming a resting potential $V_m = -43$ mV (c.f. Demarco et al., 2003). For 10 s a large net Ca²⁺ entry was induced by assuming conditions corresponding to the K8.6 medium: a depolarized membrane potential ($V_m = 0$ mV), greatly increased (39-fold) Ca²⁺ leak rate, 4.8-fold slowed PMCA, and low extracellular Na⁺. After 10 s, the conditions were changed to mimic the supposed effect of each test solution during recovery: normal membrane potential and leak but 79% depressed PMCA, or no Na⁺ outside, or no operation of the MCU. These calculations generated the simulated time courses of [Ca²⁺]ᵢ in Fig. 9 B.
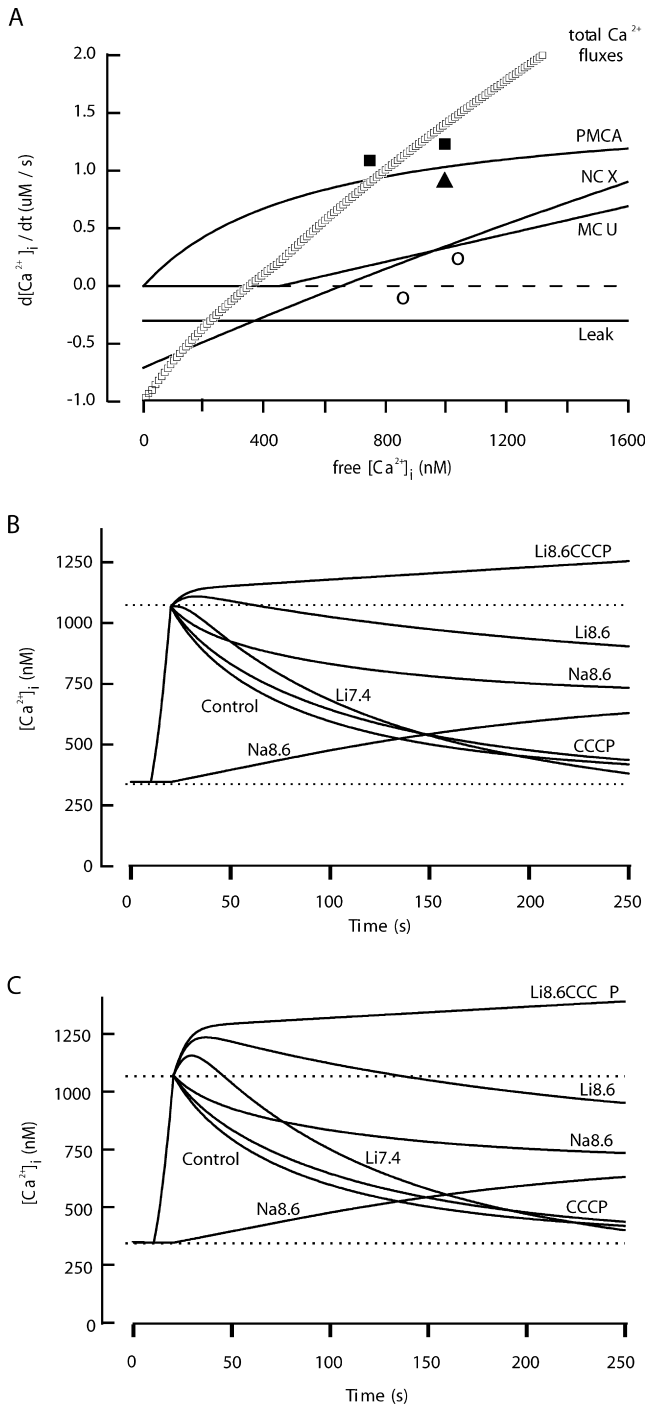
Since under control conditions the postulated [Ca²⁺]ᵢ dependence of the total flux (curve labeled "Total Ca²⁺ fluxes" in Fig. 9 A) is nearly linear, the model predicts an exponential decay of [Ca²⁺]ᵢ after an imposed load. The calculated recovery time constant is 63 s for the standard conditions. To simulate the physiological condition where there is no indo-1 in the cell, we repeated the calculation setting the indo-1 concentration to zero and obtained a decay time constant of 44 s. Without the buffering effect of indo-1, the peak [Ca²⁺]ᵢ during the simulated 10-s depolarization reached 1.84 μM.

Many qualitative features of the experiments in Figs. 3, 5, 6, and 7 were captured in the simulations (Fig. 9 B). These include: a nearly exponential normal clearance time course, slowed and incomplete clearance when the PMCA is slowed (Na8.6), a [Ca²⁺]ᵢ rise in Na8.6 even without depolarization, a delayed but nearly complete clearance in Li7.4, much less recovery in Li8.6, a minor effect of NaCCP7.4, and no net clearance in LiCCP8.6. Another striking feature is a post-depolarization [Ca²⁺]ᵢ rise whenever the Na⁺ is re-

placed by Li⁺. This rise occurs because the NCX runs transiently in reverse in a Na⁺-free extracellular medium so long as there is Na⁺ inside the sperm. However, comparison to the experiments shows some quantitative differences. The most obvious is that the simulated postdepolarization rise in Li⁺ had a lower amplitude than we observed.

In the model, the resting [Ca²⁺]ᵢ is the level where total calcium fluxes go to 0—near 350 nM in Fig. 9 A. At this level, the PMCA is quite actively exporting Ca²⁺, and the leak and the NCX are bringing Ca²⁺ into the cell. Thus, the model postulates a dynamic balance of influxes and effluxes that would be sensitive to changes in any of these mechanisms. Particularly, the NCX is sensitive to changes of [Na⁺] in two ways. First, because of a third-power dependence on [Na⁺]ᵢ, the reversal potential and the "reversal [Ca²⁺]ᵢ" at fixed potential of the NCX shift dramatically with small changes of [Na⁺]ᵢ. Second, the NCX undergoes a rapid and reversible inactivation (sometimes called "gating") that depends on the ionic conditions (Matsuoka and Hilgemann, 1994). We now speculate on possible consequences of these two features.

Our results show that the [Ca²⁺]ᵢ baseline level and the amplitude of the KCl-evoked [Ca²⁺]ᵢ transient became progressively higher during the experiment. For example, in Fig. 2 the [Ca²⁺]ᵢ level just before each of the five depolarizations is 95, 260, 360, 400, and 425 nM, respectively, and the KCl-evoked step change (Δ[Ca²⁺]ᵢ) was 366, 818, 1,250, 1,187, and 1,115 nM. Such changes can be mimicked in the model by making any of several simple changes after each trial: increasing the resting Ca²⁺ leak, increasing the [Na⁺]ᵢ, or decreasing (depolarizing) the resting membrane potential. The change of [Na⁺]ᵢ or of membrane potential would enhance the inward flow of Ca²⁺ through the NCX operating in reverse-mode at rest, thus shifting the total flux zero point and resting [Ca²⁺]ᵢ. The elevated resting [Ca²⁺]ᵢ, in turn, means that the operant calcium binding ratio is reduced (by partial titration of

A

total Ca²⁺ fluxes

PMCA

NC X

MC U

Leak

d[Ca²⁺]ᵢ / dt (uM / s)

free [Ca²⁺]ᵢ (nM)

B

Li8.6CCCP

Li8.6

Na8.6

CCCP

Li7.4

Control

Na8.6

[Ca²⁺]ᵢ (nM)

Time (s)

C

Li8.6CCC_P

Li8.6

Na8.6

CCCP

Li7.4

Control

Na8.6

[Ca²⁺]ᵢ (nM)

Time (s)

the indo-1 buffer). Relatively small changes of $[Na^+]_i$, would suffice. For example, Fig. 2 B shows a model simulation of the experiment in Fig. 2 A that assumes set points (resting levels) for $[Na^+]_i$ of 8, 13.3, 16, 17.2, 17.6, and 18 mM before the five depolarizations, respectively. Both the increasing $[Ca^{2+}]_i$ baseline and the larger $[Ca^{2+}]_i$ steps are reproduced in the simulation. Thus, small changes of $[Na^+]_i$ could explain the phenomena in our experiments, but several other explanations would be possible.

Another challenge for our simulation is to account for the large size of the extra Ca^{2+} influx when sperm are switched to Na^+-free media. The known phenomenon of ion-dependent inactivation of the NCX might be helpful in providing an explanation. The NCX rapidly goes to a lower activity, "inactivated" mode when high extracellular Na^+ causes its ion binding site(s) to face the intracellular medium (Matsuoka and Hilgemann, 1994). Despite extensive published experimentation, we cannot predict the exact inactivation status of the NCX in our experiments. Nevertheless, one tentative interpretation is that in normal physiological solutions the NCX is two-thirds inactivated and that removal of extracellular Na^+ favors a rapid recovery from this inactivation. The most elementary simulation of such events with our model would be to boost the NCX rate reversibly by a factor of three throughout each exposure to Na^+-free solutions. This is done in Fig. 9 C, which repeats the model calculations of Fig. 9 B, with a tripled NCX rate in each Na^+-free solution. The simulated overshoots of postdepolarization Ca^{2+} in Li7.4, Li8.6, and LiCCCP8.6 now have appropriate amplitudes. Such changes in the NCX rate have no effect after 30 s in these media because the $[Na]_i$ has fallen dramatically by then so the NCX has stopped transporting in either direction.

DISCUSSION

Comparison with Previous Work

Although many published studies concern Ca^{2+} elevations and their source in mammalian sperm, there is little physiological work on Ca^{2+} clearance. An old litera-

FIGURE 9. Calcium clearance calculated from a kinetic model that includes rate equations for PMCA, NCX, MCU, and Ca^{2+} leak. The assumed resting conditions include a resting membrane potential of −43 mV and a set point for $[Na^+]_i$ of 16 mM. The equations are in the APPENDIX. (A) Dependence of flux rates on $[Ca^{2+}]_i$ for each transport mechanism. Calculations assume resting levels of $[Na^+]_i$, control Na7.4 extracellular medium, and a normal resting potential. Rates would be different if any of these conditions are changed. These fluxes represent the number of micromoles of Ca^{2+} transported per second from a liter of cell water (2.3×10^{13} sperm). The rate of change of free $[Ca^{2+}]_i$ (Table I) would be given by the sum of these values (total) divided by the binding ratio for Ca^{2+}. The symbols are values estimated in Table I from our experiments (filled squares, total flux; open triangle, PMCA flux; open circles, NCX flux). (B) Calculated time courses of intracellular free $[Ca^{2+}]$ before, during, and after a simulated 10-s alkaline K^+ depolarization. To mimic the test conditions shown in Figs. 2–7, recovery parameters were changed as follows: the maximum velocity of the PMCA was reduced to 21% (for Na8.6), or $[Na^+]_o$ was set to zero (for Li7.4), or the MCU flux was turned off (for CCCP), or combinations of these changes were used. (C) The same calculation as in part B but with the velocity of the NCX increased threefold during each period in a Na^+-free, Li^+ solution to mimic possible recovery from Na^+-induced inactivation of the NCX.

ture describes the energy-linked uptake of Ca^{2+} into sperm mitochondria (e.g., Storey and Keyhani, 1974; Babcock et al., 1976) and that sperm membrane vesicles can mediate Na^+/Ca^{2+} exchange (Bradley and Forrester, 1980; Rufo et al., 1984). Several studies show that inhibitors of SERCA pumps raise $[Ca^{2+}]_i$ and can promote Ca^{2+}-mediated responses such as the acrosome reaction (e.g., Blackmore, 1993; Meizel and Turner, 1993; Trevino et al., 1998). These studies with SERCA pump inhibitors generally conclude that most of the Ca^{2+} rise occurs by Ca^{2+} entry from the outside, possibly via stores-activated plasma membrane channels (Blackmore, 1993; Jungnickel et al., 2001).

Several studies on Ca^{2+} elevations do illustrate time courses of transients, usually without analysis of the decay. For mouse sperm, $[Ca^{2+}]_i$ has been shown to decay with time constants roughly in the range from 20 to 80 s during recovery from a KCl pulse (Wennemuth et al., 2000). Similar rates of recovery were reported during the Ca^{2+} transient that occurred during application of 8-Br-cAMP (Ren et al., 2001), and in spermatogenic cells after removal of NH_4Cl solutions that elevated intracellular pH and $[Ca^{2+}]$ (Santi et al., 1998). Such observations are in good qualitative agreement with the overall clearance rates we report here.

Unexpected from our results are two reports of Ca^{2+} transients that are 1,000 times faster, coming from investigations using Ca^{2+} measurements with much higher time resolution. One of these reports (Arnoult et al., 1999) describes $[Ca^{2+}]_i$ rising at 1,000 nM/s to 9 μM and then falling with a time constant of 50 ms after rapid application of the zona-pellucida protein ZP-3 to mouse sperm. The entry is attributed to transient opening of T-type Ca^{2+} channels. The other (Suarez et al., 1993) reports that the $[Ca^{2+}]_i$ oscillates by as much as 200 nM in synchrony with the 3.5 Hz flagellar beat of hamster sperm. This oscillation would again require a time constant of Ca^{2+} removal as short as 50 ms or less. Such rapid changes of $[Ca^{2+}]_i$, if correct, could be due to readjustments of local gradients (Neher and Augustine, 1992) and millisecond equilibration with "slow" intrinsic cytoplasmic buffers (Klein et al., 1991) rather than to classical clearance of global Ca^{2+} by membrane transport mechanisms. Sea urchin sperm may also have flagellar Ca^{2+} oscillations with frequencies >1 Hz (Wood et al., 2003).

Several immunocytochemical studies localize immunoreactivity for Ca^{2+} transport molecules on mature mammalian sperm. For some of them, the absence of corroborating Western blots and of controls with absorption of the antibodies with the immunizing peptide leaves the evidence incomplete. An abundance of Ca^{2+}-permeable ion channels has been reported: several voltage-gated Ca^{2+} channels (Darszon et al., 1999; Publicover and Barratt, 1999; Westenbroek and Babcock, 1999; Wennemuth et al., 2000); cyclic nucleotide–gated channels (Walensky and Snyder, 1995; Trevino et al., 1998; Wiesner et al., 1998); IP_3 receptors but perhaps not ryanodine receptors (Ho and Suarez, 2001); the transient-receptor-potential homologue, TRPC2 (Jungnickel et al., 2001); and novel putative cation channels of the CatSper family (Quill et al., 2001; Ren et al., 2001). Each of the channels has a nonuniform distribution with specific subcellular localization, e.g., to specific domains of the sperm head or to the midpiece or principal piece of the flagellum. There is less evidence about specific transporters. Mitochondria are clearly confined to the midpiece. The only previous study of PMCA immunoreactivity found staining primarily in the postacrosomal segment of mouse sperm, with only sparse labeling in the flagellum (Adeoya-Osiguwa and Fraser, 1996), in contrast to the flagellar localization observed here (Fig. 8). An antibody against a canine NCX recognized a herring sperm protein that migrated at $\sim$120 kD on immunoblots and was localized to the sperm midpiece and flagellum (Vines et al., 2002).

Quantitative Considerations

By several criteria, Ca^{2+} movements across the resting sperm membrane are unusually small. The modeled resting leak is low, corresponding to a 2.5 fA steady inward current of Ca^{2+} and a Ca^{2+} conductance of 0.02 pS per cell (see APPENDIX). We do not know the identity of the leak channels. Likewise, the clearance mechanisms are slow, as is apparent by comparing time constants for $[Ca^{2+}]_i$ decay. Decay time constants are 40–60 s for sperm, but <3 s for chromaffin cells (Herrington et al., 1996), gonadotropes (Tse and Hille, 1992), pancreatic β cells (Chen et al., 2003), skeletal muscle (Klein et al., 1991), and heart (Bers, 2001). Our model gives the absolute fluxes per mole of cell water. For mouse sperm the PMCA is the fastest and the NCX and MCU are each about a third as fast at 1 μM Ca^{2+}, and SERCA pumping was not detected. Specifically, the transport rates at 1 μM cytoplasmic Ca^{2+} are 1.0, 0.35, 0.33, and $\sim$0 μM/s, respectively, in mouse sperm (Fig. 9 B). For rat chromaffin cells, the corresponding figures are: 8, 5, 40, and $\sim$0 μM/s; for mouse β cells: 14, 14, <4, and 38 μM/s; and for rabbit heart: 1, 30, <1, and 200 μM/s. Thus, unlike the other excitable cells, sperm are not optimized for rapid, repetitive Ca^{2+} signaling—except possibly very locally. Their global Ca^{2+} transients may rise rapidly, but then will be long lasting. The metabolic cost of their Ca^{2+} dynamics will be low (only 1 μM ATP per second for the PMCA). These findings are consistent with what we know of the final mission of mature sperm.

To translate rates of change of $[Ca^{2+}]_i$ into absolute membrane fluxes requires knowing the Ca^{2+} binding ratio. In our calculations, this binding ratio had two components. One, the exogenous component due to indo-1 dye could be calculated from measured numbers. The

other, the endogenous cytoplasmic buffer ratio, we simply assumed to be 100 in the general range found in various other cell types (Neher, 1995). If the assumed value was too high, it would not have had much effect on the derived flux rates as the indo-1 value is in the same range. However, if the assumed endogenous binding ratio was grossly too low, the flux rates would be underestimated here. Estimation of relative contributions of different clearance mechanisms would not be affected by errors in the calcium binding ratio.

An enormous amount of literature emphasizes that Ca^{2+} acts locally at high concentration near the ion channels that deliver it to the cytoplasm. This paper describes conclusions about Ca^{2+} transport obtained by looking at spatially averaged dye signals in the sperm head after we impose a Ca^{2+} load by depolarizing the cell. The 10-s depolarization must open voltage-gated Ca^{2+} channels, but which ones and where we do not know. At least five voltage-gated Ca^{2+} channel isoforms are expressed in sperm, each with its own discrete subcellular localization on parts of the head, the midpiece, or the principal piece of the flagellum (Westenbroek and Babcock, 1999; Wennemuth et al., 2000). Other putative Ca^{2+}-permeable channels are found on the flagellum as well (Ren et al., 2001; Quill et al., 2001), and we have seen that the PMCA is found primarily on the flagellum. We now need to understand compartmentalization of Ca^{2+} effects in the sperm and how local sites of entry may be coupled with local sites of action and clearance in interesting ways.

APPENDIX

This APPENDIX defines the empirical flux (M) equations for Ca^{2+} clearance used in the calculations of our model in units of total moles moved per liter per second. The units of free concentration are molar. A positive sign means Ca^{2+} removal from the cytoplasm.

$$M_{\text{leak at rest}}\ (\text{M/s}) = -0.3 \times 10^{-6}$$

$$M_{\text{leak in KCl}}\ (\text{M/s}) = 39 \times M_{\text{leak at rest}}$$

$$M_{\text{PMCA}}\ (\text{M/s}) = \{2.15 \times 10^{-6}/(1 + (550\ \text{nM}/[Ca^{2+}]_i))\}[1 + 10^{(\text{pHo} - 7.86)}]^{-1}$$

$$M_{\text{MCU}}\ (\text{M/s}) = 0\ \text{for}\ [Ca^{2+}]_i \leq 450\ \text{nM}$$

$$M_{\text{MCU}}\ (\text{M/s}) = 0.6 \times ([Ca^{2+}]_i - 450\ \text{nM})\ \text{for}\ [Ca^{2+}]_i > 450\ \text{nM}$$

$$M_{\text{NCX}}\ (\text{M/s}) = 16 \times 10^{-6}\{[Na^+]_o^3[Ca^{2+}]_i\ \exp(-0.65 \times V_m F/RT) - [Na^+]_i^3[Ca^{2+}]_o\ \exp(-0.35 \times V_m F/RT)\}/D$$

where V_m is the membrane potential and D is a denominator with many terms, given in Eq. 1 of Weber et al. (2001). The Ca^{2+} binding in sperm cytoplasm was calculated from the expression (Neher and Augustine, 1992):

$$[Ca^{2+}_{\text{bound}}]/[Ca^{2+}_{\text{free}}] = 100 + \{(c_{\text{dye}}/K_d)/(1 + [Ca^{2+}]_i/K_d)^2\},$$

where c_{dye} is the measured concentration of indo-1 dye (380 mM) and K_d is its Ca^{2+} dissociation constant (250 nM; Grynkiewicz et al., 1985). The model was solved by Euler integration in 0.5-s time steps using code written in Igor Pro. Useful conversion factors, assuming a 43-fl water volume (Du et al., 1994) and ~200 μm^2 of surface area of a mouse sperm, are that a calcium (divalent) flux of 1 $\mu mol/L$ water is equivalent to: 4.3×10^{-20} mol/s flux per sperm, 8.3 fA current per sperm, and 4.1 fA/pF current density per unit of sperm plasma membrane capacitance.

REFERENCES

Adeoya-Osiguwa, S.A., and L.R. Fraser. 1996. Evidence for Ca^{2+}-dependent ATPase activity, stimulated by decapacitation factor and calmodulin, in mouse sperm. *Mol. Reprod. Dev.* 44:111–120.

Arnoult, C., I.G. Kazam, P.E. Visconti, G.S. Kopf, M. Villaz, and H.M. Florman. 1999. Control of the low voltage-activated calcium channel of mouse sperm by egg ZP3 and by membrane hyperpolarization during capacitation. *Proc. Natl. Acad. Sci. USA.* 96:6757–6762.

Babcock, D.F., N.L. First, and H.A. Lardy. 1976. Action of ionophore A23187 at the cellular level: Separation of effects at the plasma and mitochondrial membranes. *J. Biol. Chem.* 251:3881–3886.

Babcock, D.F. 1983. Examination of the intracellular ionic environment and of ionophore action by null point measurements employing the fluorescein chromophore. *J. Biol. Chem.* 258:6380–6389.

Babcock, D.F., J. Herrington, P.C. Goodwin, Y.B. Park, and B. Hille. 1997. Mitochondrial participation in the intracellular Ca^{2+} network. *J. Cell Biol.* 136:833–844.

Babcock, D.F., and D.R. Pfeiffer. 1987. Independent elevation of cytosolic $[Ca^{2+}]$ and pH of mammalian sperm by voltage-depen-

dent and pH-sensitive mechanisms. *J. Biol. Chem.* 262:15041–15047.

Bers, D.M. 2001. Excitation-Contraction Coupling and Cardiac Contractile Force. Kluwer Academic Publishers, Dordrecht. 427 pp.

Blackmore, P.F. 1993. Thapsigargin elevates and potentiates the ability of progesterone to increase intracellular free calcium in human sperm: possible role of perinuclear calcium. *Cell Calcium.* 14:53–60.

Blaustein, M.P., and W.J. Lederer. 1999. Sodium/calcium exchange: its physiological implications. *Physiol. Rev.* 79:763–854.

Bradley, M.P., and I.T. Forrester. 1980. A sodium-calcium exchange mechanism in plasma membrane vesicles isolated from ram sperm flagella. *FEBS Lett.* 121:15–18.

Chen, L.Y., D.S. Koh, and B. Hille. 2003. Dynamics of calcium clearance in mouse pancreatic beta cells. *Diabetes.* In press.

Darszon, A., P. Labarca, T. Nishigaki, and F. Espinosa. 1999. Ion channels in sperm physiology. *Physiol. Rev.* 79:481–510.

Demarco, I.A., F. Espinosa, J. Edwards, J. Sosnik, J.L. De La Vega-Beltran, J.W. Hockensmith, G.S. Kopf, A. Darszon, and P.E. Visconti. 2003. Involvement of a Na^+/HCO^{-3} cotransporter in mouse sperm capacitation. *J. Biol. Chem.* 278:7001–7009.

DiPolo, R., and L. Beauge. 1983. The calcium pump and sodium-calcium exchange in squid axons. *Annu. Rev. Physiol.* 45:313–324.

Du, J., J. Tao, F.W. Kleinhans, P. Mazur, and J.K. Critser. 1994. Water volume and osmotic behaviour of mouse spermatozoa determined by electron paramagnetic resonance. *J. Reprod. Fertil.* 101: 37–42.

Gatto, C., and M.A. Milanick. 1993. Inhibition of the red blood cell calcium pump by eosin and other fluorescein analogues. *Am. J. Physiol.* 264:C1577–C1586.

Grynkiewicz, G., M. Poenie, and R.Y. Tsien. 1985. A new generation of Ca^{2+} indicators with greatly improved fluorescence properties. *J. Biol. Chem.* 260:3440–3450.

Gunter, T.E., L. Buntinas, G. Sparagna, R. Eliseev, and K. Gunter. 2000. Mitochondrial calcium transport: mechanisms and functions. *Cell Calcium.* 28:285–296.

Herrington, J., Y.B. Park, D.F. Babcock, and B. Hille. 1996. Dominant role of mitochondria in clearance of large Ca^{2+} loads from rat adrenal chromaffin cells. *Neuron.* 16:219–228.

Ho, H.C., and S.S. Suarez. 2001. An inositol 1,4,5-trisphosphate receptor-gated intracellular Ca^{2+} store is involved in regulating sperm hyperactivated motility. *Biol. Reprod.* 65:1606–1615.

Jungnickel, M.K., H. Marrero, L. Birnbaumer, J.R. Lemos, and H.M. Florman. 2001. Trp2 regulates entry of Ca^{2+} into mouse sperm triggered by egg ZP3. *Nat. Cell Biol.* 3:499–502.

Klein, M.G., L. Kovacs, B.J. Simon, and M.F. Schneider. 1991. Decline of myoplasmic Ca^{2+}, recovery of calcium release and sarcoplasmic Ca^{2+} pump properties in frog skeletal muscle. *J. Physiol.* 441:639–671.

Kraev, A., B.D. Quednau, S. Leach, X.F. Li, H. Dong, R. Winkfein, M. Perizzolo, X. Cai, R. Yang, K.D. Philipson, and J. Lytton. 2001. Molecular cloning of a third member of the potassium-dependent sodium-calcium exchanger gene family, NCKX3. *J. Biol. Chem.* 276:23161–23172.

Laemmli, U.K., E. Molbert, M. Showe, and E. Kellenberger. 1970. Form-determining function of the genes required for the assembly of the head of bacteriophage T4. *J. Mol. Biol.* 49:99–113.

Linck, B, Z. Qiu, Z. He, Q. Tong, D.W. Hilgemann, and K.D., Philipson. 1998. Functional comparison of the three isoforms of the Na^+/Ca^{2+} exchanger (NCX1, NCX2, NCX3). *Am. J. Physiol.* 274: C415–C423.

MacLennan, D.H., W.J. Rice, and N.M. Green. 1997. The mechanism of Ca^{2+} transport by sarco(endo)plasmic reticulum Ca^{2+}-ATPases. *J. Biol. Chem.* 272:28815–28818.

Matsuoka, S., and D.W. Hilgemann. 1992. Steady-state and dynamic properties of cardiac sodium-calcium exchange. Ion and voltage dependencies of the transport cycle. *J. Gen. Physiol.* 100:963–1001.

Matsuoka, S., and D.W. Hilgemann. 1994. Inactivation of outward Na^+-Ca^{2+} exchange current in guinea-pig wetricular myocytes. *J. Physiol.* 476:443–458.

Meizel, S., and K.O. Turner. 1993. Effects of polyamine biosynthesis inhibitors on the progesterone-initiated increase in intracellular free Ca^{2+} and acrosome reactions in human sperm. *Mol. Reprod. Dev.* 34:457–465.

Neher, E. 1995. The use of fura-2 for estimating Ca buffers and Ca fluxes. *Neuropharmacology.* 34:1423–1442.

Neher, E., and G.J. Augustine. 1992. Calcium gradients and buffers in bovine chromaffin cells. *J. Physiol.* 450:273–301.

Okamura, N., Y. Tajima, A. Soejima, H. Masuda, and Y. Sugita. 1985. Sodium bicarbonate in seminal plasma stimulates the motility of mammalian spermatozoa through direct activation of adenylate cyclase. *J. Biol. Chem.* 260:9699–9705.

O'Toole, C.M., C. Arnoult, A. Darszon, R.A. Steinhardt, and H.M. Florman. 2000. Ca^{2+} entry through store-operated channels in mouse sperm is initiated by egg ZP3 and drives the acrosome reaction. *Mol. Biol. Cell.* 11:1571–1584.

Philipson, K.D., and D.A. Nicoll. 2000. Sodium-calcium exchange: a molecular perspective. *Annu. Rev. Physiol.* 62:111–133.

Publicover, S.J., and C.L. Barratt. 1999. Voltage-operated Ca^{2+} channels and the acrosome reaction: which channels are present and what do they do? *Hum. Reprod.* 14:873–879.

Quednau, B.D., D.A. Nicoll, and K.D. Philipson. 1997. Tissue specificity and alternative splicing of the Na^+/Ca^{2+} exchanger isoforms NCX1, NCX2, and NCX3 in rat. *Am. J. Physiol.* 272:C1250–C1261.

Quill, T.A., D. Ren, D.E. Clapham, and D.L. Garbers. 2001. A voltage-gated ion channel expressed specifically in spermatozoa. *Proc. Natl. Acad. Sci. USA.* 98:12527–12531.

Ren, D., B. Navarro, G. Perez, A.C. Jackson, S. Hsu, Q. Shi, J.L. Tilly, and D.E. Clapham. 2001. A sperm ion channel required for sperm motility and male fertility. *Nature.* 413:603–609.

Rufo, G.A., P.K. Schoff, and H.A. Lardy. 1984. Regulation of calcium content in bovine spermatozoa. *J. Biol. Chem.* 259:2547–2552.

Santi, C.M., T. Santos, A. Hernandez-Cruz, and A. Darszon. 1998. Properties of a novel pH-dependent Ca^{2+} permeation pathway present in male germ cells with possible roles in spermatogenesis and mature sperm function. *J. Gen. Physiol.* 112:33–53.

Shimizu, H., M.L. Borin, and M.P. Blaustein. 1997. Use of La^{3+} to distinguish activity of the plasmalemmal Ca^{2+} pump from Na^+/Ca^{2+} exchange in arterial myocytes. *Cell Calcium.* 21:31–41.

Storey, B.T., and E. Keyhani. 1974. Energy metabolism of spermatozoa: III. Energy-linked uptake of calcium ion by the mitochondria of rabbit epididymal spermatozoa. *Fertil. Steril.* 25:976–984.

Su, Y.H., and V.D. Vacquier. 2002. A flagellar K^+-dependent Na^+/Ca^{2+} exchanger keeps Ca^{2+} low in sea urchin spermatozoa. *Proc. Natl. Acad. Sci. USA.* 99:6743–6748.

Suarez, S.S., S.M. Varosi, and X. Dai. 1993. Intracellular calcium increases with hyperactivation in intact, moving hamster sperm and oscillates with the flagellar beat cycle. *Proc. Natl. Acad. Sci. USA.* 90:4660–4664.

Trevino, C.L., C.M. Santi, C. Beltran, A. Hernandez-Cruz, A. Darszon, and H. Lomeli. 1998. Localisation of inositol trisphosphate and ryanodine receptors during mouse spermatogenesis: possible functional implications. *Zygote.* 6:159–172.

Tse, A., and B. Hille. 1992. GnRH-induced Ca^{2+} oscillations and rhythmic hyperpolarizations of pituitary gonadotropes. *Science.* 255:462–464.

Vines, C.A., K. Yoshida, F.J. Griffin, M.C. Pillai, M. Morisawa, R. Yanagimachi, and G.N. Cherr. 2002. Motility initiation in herring sperm is regulated by reverse sodium calcium exchange. *Proc. Natl. Acad. Sci. USA.* 99:2026–2031.

Visconti, P.E., J.L. Bailey, G.D. Moore, D. Pan, P. Olds-Clarke, and G.S. Kopf. 1995. Capacitation of mouse spermatozoa. I. Correlation between the capacitation state and protein tyrosine phosphorylation. *Development.* 121:1129–1137.

Walensky, L.D., and S.H. Snyder. 1995. Inositol 1,4,5-trisphosphate receptors selectively localized to the acrosomes of mammalian sperm. *J. Cell Biol.* 130:857–869.

Weber, C.R., K.S. Ginsburg, K.D. Philipson, T.R. Shannon, and D.M. Bers. 2001. Allosteric regulation of Na/Ca exchange current by cytosolic Ca in intact cardiac myocytes. *J. Gen. Physiol.* 117:119–131.

Wennemuth, G., A.E. Carlson, A.J. Harper, and D.F. Babcock. 2003. Bicarbonate actions on flagellar and calcium channel responses: initial events in sperm activation. *Development.* 130:1317–1326.

Wennemuth, G., R.E. Westenbroek, T. Xu, B. Hille, and D.F. Babcock. 2000. $Ca_V2.2$ and $Ca_V2.3$ (N- and R-type) Ca^{2+} channels in depolarization- evoked entry of Ca^{2+} into mouse sperm. *J. Biol. Chem.* 275:21210–21217.

Westenbroek, R.E., and D.F. Babcock. 1999. Discrete regional distributions suggest diverse functional roles of calcium channel $\alpha 1$ subunits in sperm. *Dev. Biol.* 207:457–469.

Wiesner, B., J. Weiner, R. Middendorff, V. Hagen, U.B. Kaupp, and I. Weyand. 1998. Cyclic nucleotide-gated channels on the flagellum control Ca^{2+} entry into sperm. *J. Cell Biol.* 142:473–484.

Wood, C.D., A. Darszon, and M. Whitaker. 2003. Speract induces calcium oscillations in the sperm tail. *J. Cell Biol.* 161:89–101.

Xu, W., B.J. Wilson, L. Huang, E.L. Parkinson, B.J. Hill, and M.A. Milanick. 2000. Probing the extracellular release site of the plasma membrane calcium pump. *Am. J. Physiol. Cell Physiol.* 278:C965–C972.